IEEE Access
Multidisciplinary | Rapid Review | Open Access Journal

Received July 27, 2019, accepted August 5, 2019, date of publication August 14, 2019, date of current version August 31, 2019.

Digital Object Identifier 10.1109/ACCESS.2019.2935344

Control and Optimization of Residential Photovoltaic Power Generation System With High Efficiency Isolated Bidirectional DC–DC Converter

RUI LI, (Member, IEEE), AND FANGYUAN SHI

Key Laboratory of Control of Power Transmission and Conversion, Ministry of Education, School of Electronic Information and Electrical Engineering, Shanghai Jiao Tong University, Shanghai 200240, China

Corresponding author: Rui Li (liruiqd@sjtu.edu.cn)

This work was supported in part by the National Key Research and Development Project under Grant 2018YFB1500702, and in part by the National Natural Science Foundation of China under Grant 51777124.

ABSTRACT Currently, residential photovoltaic power generation system is increasingly used worldwide. In this paper, an optimized structure of residential photovoltaic (PV) power generation system with 1500V DC bus is proposed. It includes PV panels, a three-level boost converter, a high efficiency isolated bidirectional DC-DC converter, battery and three-phase five-level DC-AC converter that can work under islanding mode or grid-connected mode. The higher DC bus voltage greatly reduces line loss and improves efficiency of the system. An energy management scheme used for the system is proposed in this paper to guarantee the stability of the system and to increase its economic benefits. Besides, the optimized method for the structure of the bidirectional dc-dc converter is proposed. This structure can achieve higher DC voltage gain and higher efficiency. Furthermore, for low voltage battery application in the residential system, LLC and CLLC under DC transformer (DCX) mode are evaluated and the LLC is selected as the isolated bidirectional DC-DC converter. The optimized designed method of bidirectional LLC is proposed. Finally, experiments are carried out to verify the performance of the optimized converters and the system.

INDEX TERMS Energy management scheme, high efficiency, isolated bidirectional DC-DC converter, LLC converter, residential photovoltaic power generation system.

I. INTRODUCTION

Since photovoltaic power generation system can alleviate energy crisis and reduce environmental pollution, it has been applied worldwide [1].

Residential photovoltaic power generation system is increasingly applied to houses [2], [3]. Residential photovoltaic power generation system is aimed to provide continuous and reliable power supply to household loads [4]. It is an active distributed network employing PV panels, battery energy storage system (BESS) and variety of converters and loads, operated grid-connected or islanded, in a controlled, coordinated way [5].

Since the PV panels' output power is irregular and stochastic due to the intermittent nature of the sun irradiation, there are still some problems such as load mismatch, poor load flowing, voltage instability and reliability problems. Therefore, BESS is necessary in the residential photovoltaic power generation system [1].

In the traditional PV power generation system, BESS is always connected to the DC bus directly. However, there are some potential dangers for batteries when the load changes suddenly without current control. So, it is necessary to insert a bidirectional DC-DC converter between the DC bus and batteries to control the discharging current [6].

Besides, the traditional PV system with single DC-AC converter is not suitable for the residential situation for its higher economic cost and complex maximum power point tracking (MPPT) control [7], [8]. The additional MPPT stage is believed as a better way to address the problems of voltage instability of PV panels. With the development of wide band gap devices, SiC devices can be used in the 1500V DC

The associate editor coordinating the review of this article and approving it for publication was Bin Zhou.

bus to reduces line loss and improve the efficiency of the system.

According to whether connected to the grid, residential photovoltaic power generation system can be divided into grid-tied system and stand-alone system [9]. Energy consumption and cost are important factors in such a system because they directly affect the resource utilization and economic benefits of the system [10]. Therefore, grid-tied residential photovoltaic power generation system is preferred because it can not only ensure the reliability of power supply but also benefit the residents via taking the advantage of the time-of-use (ToU) price [11].

In conclusion, residential photovoltaic power generation system is a complex system including PV panels, BESS, DC-DC converters and DC-AC converters. Therefore, coordination among the various components in the system is very important. It means that the energy management scheme is necessary since there are three different converters influencing the DC bus voltage and the energy transmission [12]. Besides, the costs and the economic benefits should also be considered in the energy management scheme.

Therefore, the optimization of residential photovoltaic power generation system must take the factors discussed above into account. This paper dedicates to optimizing the residential photovoltaic power generation system to achieve higher efficiency and higher economic benefits.

In this paper, the contributions can be concluded as

1) The optimized structure of the system oriented to 1500V DC bus is proposed. The higher DC bus voltage greatly reduces line loss and improves efficiency of the system.
2) An energy management scheme is proposed. It is aimed to improve the reliability of power supply and to increase the economic benefits of the system. The scheme ensures the reliability of power supply for the residential load and increases the economic benefits via feeding back energy to the grid.
3) The optimized method for the structure of bidirectional DC-DC converter is proposed. The structure that battery side is parallel connected and bus side series connected can easily achieve higher DC voltage gain and higher efficiency, and improve the energy utilization of the system.
4) The LLC and CLLC under DCX mode are evaluated. The optimized design method is proposed. Theoretical analysis and experimental results show that optimized bidirectional LLC has more advantages in low-voltage applications.

Thus, the rest of this paper is organized as follows. Section II reviews the related works. Section III introduces the proposed energy management scheme used for the residential situation aimed to guarantee the reliability and efficiency of the system. Section IV discusses the structure of isolated bidirectional DC-DC converter with high efficiency and high DC gain and evaluates the performance of LLC and CLLC in lower voltage situation. Section V gives experimental results and analysis. Finally, section VI draws the conclusion.

II. RELATED WORKS

Considering that this study involves optimizing the whole PV system in residential situation, related works are reviewed by several sections including PV system and energy management scheme, DC-DA converters and DC-DC converters.

A. PV SYSTEM AND ENERGY MANAGEMENT SCHEME

Considering the MPPT, a two-stage grid-connected PV system with an adjustable dc-link voltage is proposed, wherein MPPT is realized by DC-DC converters and great performance is achieved [13]. However, there is no BESS in the system. The irregularity and randomness of solar irradiation will lead to the frequent interaction between the system and power grid. In [9], a PV system with BESS was proposed and an energy management scheme based on the DC bus signaling is given. The system can achieve higher resource utilization and higher reliability. But only the DC load is considered in the system. It is not suitable for the residential situation. In [14], a residential PV system with grid-tied three phase converter is presented and an optimized energy management scheme is proposed. The system can achieve ''Plug and Play'' in residential situation. Nevertheless, the energy management scheme only focuses on the reduction of the reaction with the grid. The economic benefits are ignored. Besides, in energy management scheme, the state of charge (SOC) of the battery is a very important variation in energy management. However, SOC for batteries are usually ignored in the energy management scheme [9], [15].

B. DC-AC CONVERTERS

For three phase grid-tied system, traditional two-level inverters have been used in the system for their simplicity [16]. However, these two-level inverters require large filter and high-voltage-rated semiconductor devices, which leads to low power density and large power loss [17]. To obtain smaller filter size and higher efficiency, multilevel inverters were introduced to the photovoltaic power generation system. Then, a three-level single-phase inverter and a three-level three-phase inverter were used in the photovoltaic power generation systems respectively to achieve higher efficiency, lower THD and lower EMI noise [18], [19]. Three-phase five-level inverter based on SiC devices and interleaved three-level T-type inverters were used in PV systems and obtained high efficiency and high power-density [20]. With the development of SiC devices, higher DC bus voltage and multi-level inverters can improve the efficiency. However, the DC bus voltage of these systems are still 850V.it means that the system efficiency can be further improved. In fact, SiC devices can be used in 1500V DC bus easily to improve the efficiency of the system significantly.

C. DC-DC CONVERTERS

For 1500V DC bus, a DC-DC converter is needed between PV panels and inverter to avoid too much number of series-connected PV panels and achieve MPPT. Besides, an isolated bidirectional DC-DC converter between the DC bus and batteries is more important in the residential photovoltaic power generation system to provide electrical isolation.

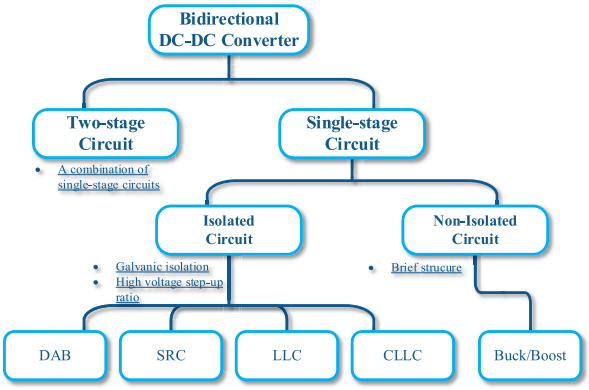

FIGURE 1. Classification diagram of bidirectional DC-DC converters.

The map of bidirectional DC-DC converter has been shown in Fig. 1. In [21], a bidirectional buck/boost circuit was directly used in a photovoltaic energy storage system. However, in residential utilization, for safety consideration, the voltage rating of battery module is normally below 48V, which means that the converter between battery and DC bus (voltage rating is up to 1500V for three-phase five-level inverter) needs to meet high voltage gain requirement that non-isolated topology is difficult to achieve. Hence, isolated topology is preferred for its higher DC voltage gain and electrical isolation [22]. To achieve higher efficiency and better EMI performance, technologies that can achieve soft-switching are best choice as isolated converter in the residential photovoltaic power generation system. These topologies include dual active bridge (DAB), series resonant converter (SRC), LLC converter and CLLC converter. DAB has received extensive attention in recent years, and has been applied more and more in energy storage system and microgrid. Its primary side can achieve zero voltage switching (ZVS) turn-on under certain load conditions. However, the phase difference between voltage and current will result in a larger cycle power, which limits the further improvement of efficiency and power density [23], [24]. SRC is a widely used bidirectional DC-DC converter as well. Since there are only two series resonant elements in SRC, the voltage gain cannot exceed 1. At the same time, SRC cannot achieve soft switching in all gain ranges, and the large switching loss makes it difficult to improve efficiency [25], [26]. LLC is very suitable for applications that require high efficiency and high power density since it can realize ZVS on the primary side and ZCS on the secondary side. Besides, the voltage gain of LLC can exceed 1, that is, the converter can operate in step-down mode and step-up mode. In fact, LLC is still working as SRC under backward condition, and its equivalent output gain is smaller than 1 [27]. Although the π-type LLC converter can amplify the gain range of the converter under bidirectional operation and have no effect on the soft-switching realization of the circuit, the reactive power of the circuit is greatly increased [28]. Therefore, it is not suitable for high efficiency application. CLLC can also realize ZVS-on at primary side and ZCS-off at secondary side in full load range. At the same time, operation conditions of the converter under forward and backward mode are the same. However, it is difficult to control because there are two resonant peaks in its gain curve [29], [30]. Additionally, the step-up ratio of DC voltage is up to 31.25, which is too high to realize in a single-stage circuit. Then, two-stage circuit was proposed. A two-stage bidirectional DC-DC converter based on LLC and interleaved boost converter were used in a charger. This converter works as a one-stage DC-DC converter (LLC only) in charging mode and two-stage in discharging mode [31]. To reduce the operation frequency range and obtain wide DC gain range, a bidirectional DC-DC converter based on LLC and buck/boost was proposed in a photovoltaic energy storage system [22].

D. CONTRIBUTIONS

PV power generation system can effectively alleviate energy crisis and reduce environmental pollution. Unlike the related works reviewed above, this paper dedicates to optimize the residential photovoltaic power generation system to achieve higher efficiency and higher economic benefits.

The contribution of this paper is mainly manifested in two aspects:

1) Higher efficiency: to achieve higher efficiency, the optimized structure of the system with1500V DC bus which is rarely employed is used. To improve the efficiency of the system, optimized method for the structure of bidirectional DC-DC converter is proposed. CLLC and LLC used in the residential situation are evaluated. The better choice is given and optimized design method is proposed.
2) Higher economic benefits: to increase the reliability and economic benefits in the residential situation, an energy management scheme is proposed. Users can get more economic benefits from ToU tariff.

III. ENERGY MANAGEMENT SCHEME OF OPTIMIZED SYSTEM

A. SYSTEM CONFIGURATION

The optimized residential photovoltaic power generation system has been shown in Fig. 2. A three-level boost, an isolated bidirectional DC-DC converter and a three-phase five-level DC-AC converter share a DC bus. DC-AC converter, grid and residential load share an AC bus. PV panels only transfer the power to the DC bus via a three-level boost converter. The isolated bidirectional DC-DC converter is a

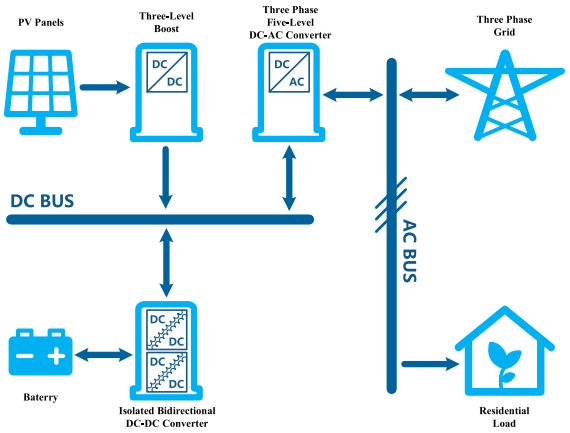

FIGURE 2. The optimized residential PV power generation system.

key element connected with battery and DC bus to balance the power differences between PV panels and residential load. The three-phase five-level DC-AC converter is connected between DC bus and AC bus, which enables bidirectional power flow to improve the system reliability.

Since the proposed energy management scheme is designed for the residential photovoltaic power generation system, reliability is the most important standard for the scheme. Then the proposed energy management scheme is aimed to enhance the system reliability with consideration of economic benefits.

B. ENERGY MANAGEMENT SCHEME

In this section, an energy management scheme is proposed for the residential power generation system to ensure the power balance and reliability of the system and increase the economic benefits. As shown in Fig. 3, the energy management scheme is based on the ''Self-produced and Self-used.'' The PV panels have the highest priority in power supply.

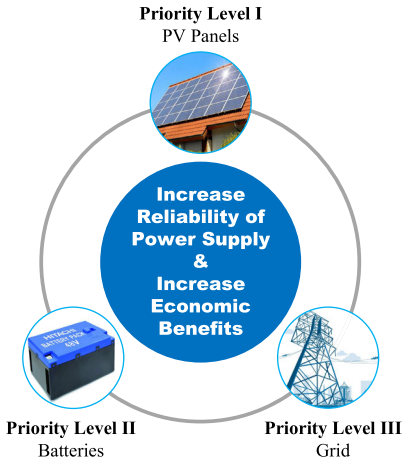

FIGURE 3. Priority in power supply of the optimized system.

To obtain more economic benefits and maintain the reliability of the system, the consideration of sunshine time and ToU tariff is added to the design of energy management scheme. Since sunshine hours and ToU tariff are completely different in different regions, the design and analysis in this section are all based on Shanghai, China.

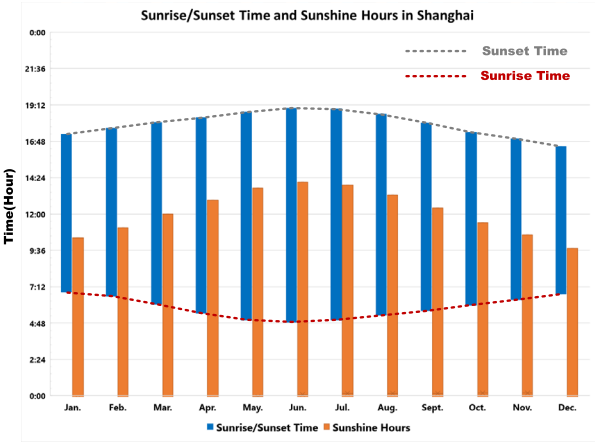

FIGURE 4. Sunrise time, sunset time and sunshine hours of Shanghai in different months.

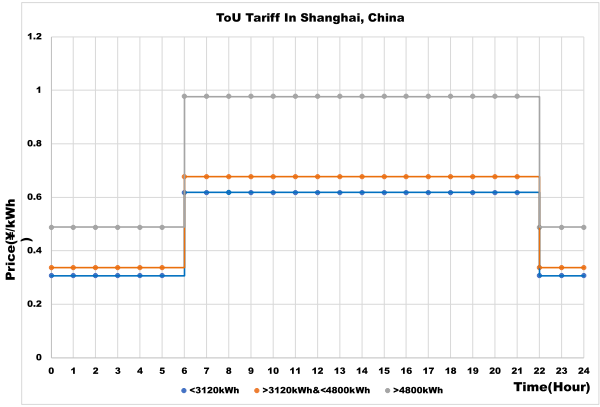

FIGURE 5. The ToU tariff in Shanghai.

The sunrise time, sunset time and sunshine hours of Shanghai in different months have been shown in Fig. 4. The ToU tariff in Shanghai is shown in Fig. 5. In Shanghai, sunrise time is near six o'clock which is one of the boundaries of ToU tariff. Unlike the sunrise time, sunset time in Shanghai is long before another boundary. Besides, the average sunlight hours in different month in Shanghai are different. To improve the resource utilization, this difference in different month must be considered. Since the peak time is from 6:00-22:00, to pursue the highest economic benefits, at different boundaries the system must be switched to the different operation mode. Then the proposed energy management scheme can be divided into three main modes, MODE1, MODE2 and MODE3, as shown in Fig. 6. These three main modes are identified by the sunrise time, sunset time and the boundary of peak time and valley time. In each main mode, the operation can be divided into several sub-modes and the state machine has been shown in

TABLE 1. Operation mode of the proposed energy management scheme.

	MODE1 (Sunrise Time – Sunset Time)		MODE2 (Sunset Time – 22:00)	MODE3 (22:00 – Sunrise Time)
SOC of battery	$P_{PV} \geq P_{LOAD}$	$P_{PV} < P_{LOAD}$	$P_{PV} < P_{LOAD}$	$P_{PV} < P_{LOAD}$
$SOC \leqslant SOC_{min}$	MODE1A UD2D: MPPT BD2D: Step-up D2A: Islanding	MODE1D UD2D: MPPT BD2D: Step-down D2A: Turn off	MODE2B UD2D: Turn off BD2D: Turn off D2A: Grid connection	MODE3A UD2D: Turn off BD2D: Step-down D2A: Grid connection
$SOC_{min} < SOC < SOC_{max}$	MODE1A UD2D: MPPT BD2D: Step-up D2A: Islanding	MODE1C UD2D: MPPT BD2D: Step-up D2A: Islanding	MODE2A UD2D: Turn off BD2D: Step-up D2A: Islanding	MODE3A UD2D: Turn off BD2D: Step-down D2A: Grid connection
$SOC \geqslant SOC_{max}$	MODE1B UD2D: MPPT BD2D: Turn off D2A: Grid connection	MODE1C UD2D: MPPT BD2D: Step-up D2A: Islanding	MODE2A UD2D: Turn off BD2D: Step-up D2A: Islanding	MODE3A UD2D: Turn off BD2D: Step-down D2A: Grid connection

UD2D = Unidirectional DC-DC converter, BD2D = Bidirectional DC-DC converter, D2A = DC-AC converter

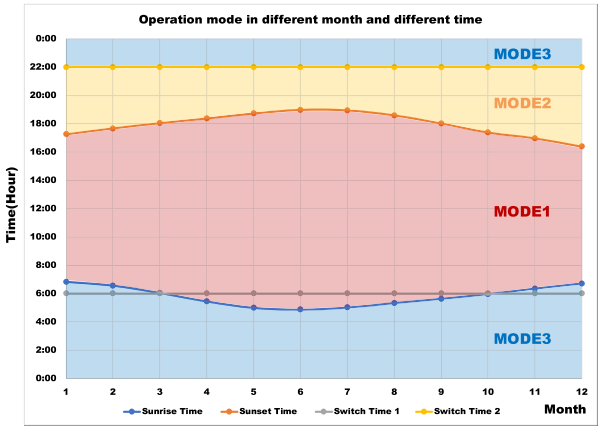

FIGURE 6. Switching time of three main modes according to the sunrise time, sunset time and ToU tariff.

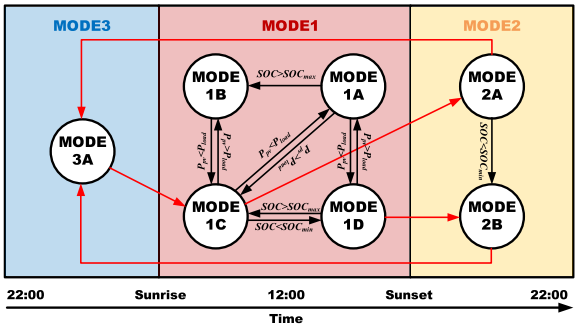

FIGURE 7. State machine of the operating modes.

Fig. 7. In Fig. 7, the switching of MODE1, MODE2 and MODE3 are controlled by the preset time based on the actual month. The red lines represent the switching of sub-modes when the main mode is switched.

In each main mode, sub-modes are identified by the maximal output power of PV panels P_{PV}, SOC of battery and load power P_{LOAD}. Then, the sub-mode selection can follow the rules shown in TABLE 1. In which, SOC_{min} is the low limit of SOC and is SOC_{max} high limit. SOC_{max} and SOC_{min} are set as 95% and 5% to prevent battery from over-charging or over-discharging. Each sub-mode is described as follows and the schematic diagram of power flow is shown in Fig. 8.

MODE1A: As shown in Fig. 8(a), if the load power is less than the power PV panels generated and the battery is not fully charged, that is $P_{PV} \geq P_{LOAD}$ and $SOC \leq 95\%$, the PV panels are the main power supply. Then, the unidirectional DC-DC converter operates at MPPT mode, the bidirectional DC-DC converter operates at step-up mode to maintain the DC bus voltage, and no power is obtained from the grid.

MODE1B: As shown in Fig. 8(b), if the load power is less than the power PV panels generated and the battery is fully charged, that is $P_{PV} \geq P_{LOAD}$ and $SOC \geq 95\%$, the PV panels are the main power supply. To pursue the higher economic benefits in the residential system, the excess energy will be fed to the grid. Then the DC bus voltage will be controlled by DC-AC converter and the bidirectional DC-DC converter will be turned off.

MODE1C: As shown in Fig. 8(c), if the load power is greater than the power PV panels generated and the battery is not fully discharged, that is $P_{PV} < P_{LOAD}$ and $SOC > 5\%$, both BESS and PV panels are the power supply. Then, the bidirectional DC-DC converter operates at step-up mode to control the DC bus voltage and transfer power to the load and the unidirectional DC-DC converter will operate at MPPT mode. The grid is not connected at this mode.

MODE1D: As shown in Fig. 8(d), if the load power is greater than the power PV panels generated and the battery is fully discharged, that is $P_{PV} < P_{LOAD}$ and $SOC < 5\%$, the grid has to be connected as main power supply. Then, the DC-AC converter is turned off to prevent batteries from charging by the grid. Unidirectional DC-DC converter switches to constant voltage (CV) mode to maintain the DC

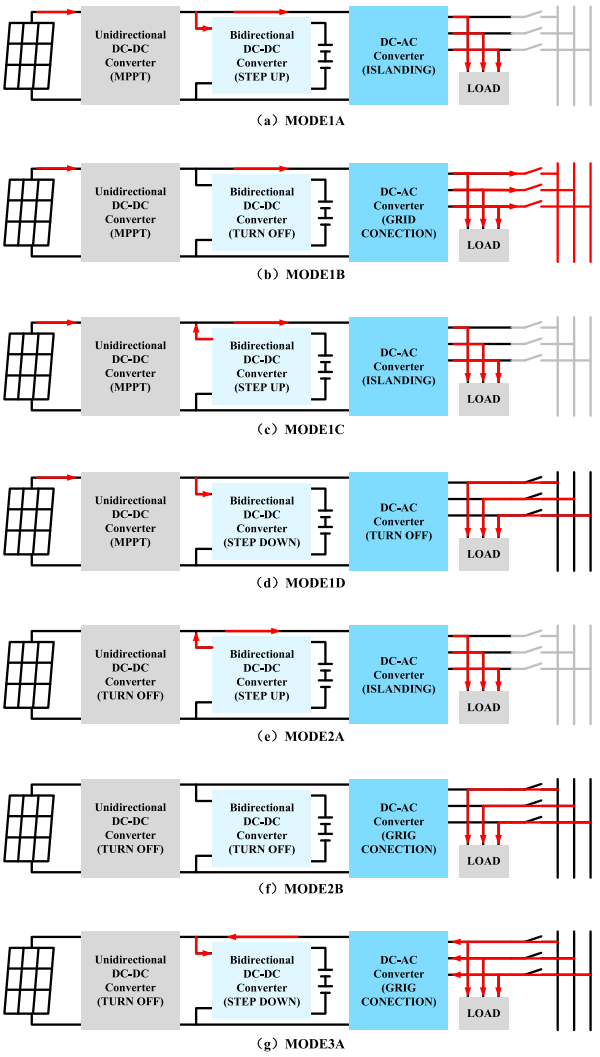

FIGURE 8. Schematic diagram of power flow of each sub-mode.

bus voltage and charge the batteries. Then, batteries can be charged by PV panels only and cost can be reduced. Besides, MODE1D will not switch to MODE1C until the $SOC \geq 95\%$.

MODE2A: As shown in Fig. 8(e), MODE2A is the same as MODE1C except that the unidirectional DC-DC converter is turned off. The bidirectional DC-DC converter operates at step-up mode to control the DC bus voltage and transfer power to the load as power supply. The grid is not connected at this mode.

MODE2B: As shown in Fig. 8(f), MODE2B is similar to the MODE1D. If $P_{PV} < P_{LOAD}$ and $SOC < 5\%$, the grid has to be connected as main power supply. Unlike MODE1D, the PV panels can not work in MODE2. To reduce the higher electricity cost caused by peak time price and increase the economic benefits, the batteries are not allowed to be charged.

MODE3A: As shown in Fig. 8(g), only one sub-mode in MODE3. Since BESS is the main power supply in MODE2 and valley time price is much lower than peak time price, the grid becomes the unique power supply. The unidirectional DC-DC converter operates at step-down mode to charge the batteries. The energy stored in the BESS will be used as main power supply to replace the grid in next morning.

C. CONTROL METHODS

The control methods corresponding to the proposed energy management system has been shown in Fig. 9. In which, D_1^* is the reference duty cycle of the unidirectional DC-DC converter, D_2^* is the reference duty cycle of the bidirectional DC-DC converter and D_3^* is the reference duty cycle of the DC-AC converter.

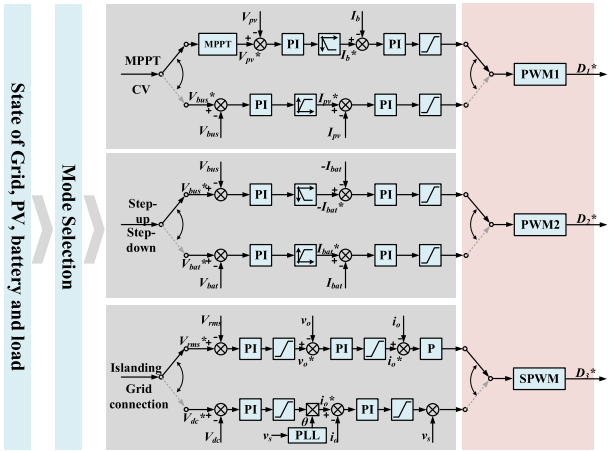

FIGURE 9. Control diagram of the residential photovoltaic power generation system.

The three-level boost converter is employed in tracking maximum power point in the system. The three-level boost converter can operate at MPPT mode or CV mode. Perturbations method is used here to achieve MPPT, in which V_{pv} and I_{pv} are the voltage and current of the PV panels, V_{pv}^* is the reference voltage of V_{pv}, I_b^* and I_b are the reference current and actual current of the three-level boost. For CV mode, V_{bus} is voltage of DC bus, V_{bus}^* is the reference voltage of V_{bus} as outer loop reference and the inner loop reference is I_{pv}^*, the reference of PV panels current I_{pv}.

A two-stage isolated bidirectional DC-DC converter is used to control the voltage and current of the battery. This DC-DC converter can operate in step-up mode or step-down mode. Since the bidirectional LLC works as a DCX, just the duty cycle of the buck/boost is controlled in the bidirectional DC-DC converter. When it works in step-up mode, a double closed loop control is applied. In which V_{bus}^* is the reference of outer loop and the inner loop reference is $-I_{bat}^*$, the reference of battery current I_{bat}. When it works in step-down mode, V_{bat} is voltage of battery, V_{bat}^* is reference voltage of V_{bat} as outer loop reference and the inner loop reference is I_{bat}^*. Then the reference duty cycle for bidirectional DC-DC converter can be obtained in different operation mode.

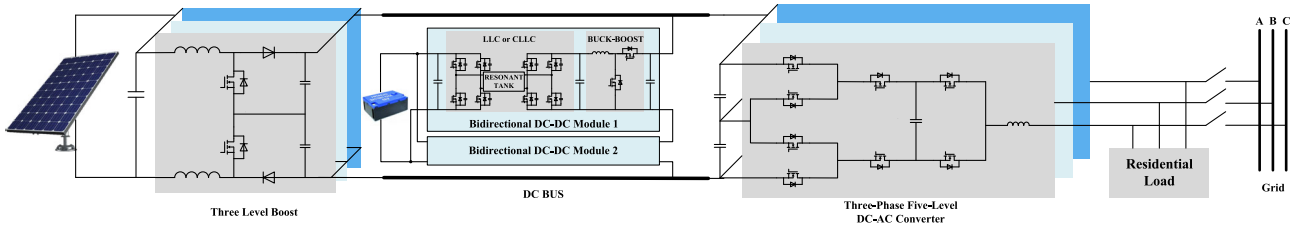

FIGURE 10. Configuration of the proposed residential photovoltaic power generation system.

A three-phase five-level inverter is used which can operate in islanding mode or grid connection mode. In islanding mode, the DC-AC converter works as a stand-alone inverter. A triple loop control is used in which V_{rms} is the RMS of output voltage and V^*_{rms} is its reference, v_o and v^*_o are instantaneous output voltage and its reference and i_o and i^*_o are instantaneous output current and its reference calculated via voltage loop. In grid connection mode, the DC-AC converter has to maintain the voltage of DC bus, so the outer loop reference is replaced by DC side voltage. Besides, to connect the grid, the grid voltage V_s is sampled to calculated its phase angle θ. Then, the SPWM signal is generated to control the AC or DC voltage.

IV. OPTIMIZATION OF HIGH EFFICIENCY ISOLATED BIDIRECTIONAL DC-DC CONVERTER

A. CONFIGURATION OF ISOLATED BIDIRECTIONAL DC-DC CONVERTER

In this section, the high efficiency isolated bidirectional DC-DC converter is discussed. This bidirectional DC-DC converter is very important in the residential photovoltaic power generation system as shown in the Fig. 10. For safety consideration, the battery voltage is always lower than 48V. It means that a high voltage gain is required since the DC bus voltage is up to 1500V. To improve the DC gain and achieve higher efficiency, an optimized isolated bidirectional DC-DC converter is shown in Fig. 11. The converter consists of two identical independent modules. The module is a two-stage isolated bidirectional DC-DC converter, in which a bidirectional LLC or CLLC can be employed in providing electrical isolation and higher DC gain. To achieve higher efficiency, the isolated bidirectional DC-DC converter works as a DCX and a buck/boost is added to improve the DC gain range of the module. Since the voltage of battery side is very low compared to the voltage of DC bus, the current is large so that the problems caused by large current and power loss are prominent. To avoid these problems, a scheme that battery side connected in parallel and DC bus side connected in series is adopted, which is beneficial to higher efficiency and higher DC gain.

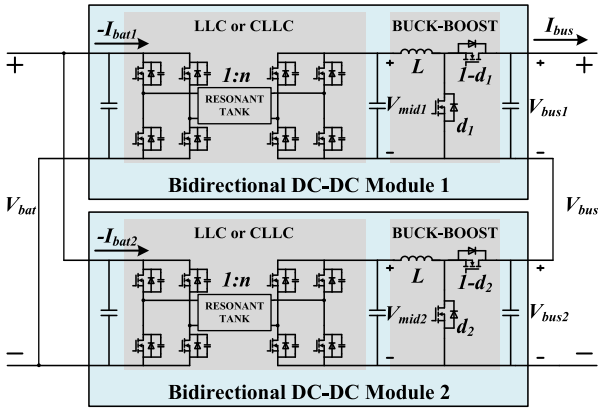

FIGURE 11. Configuration of isolated bidirectional DC-DC converter in the proposed system.

There are some advantages for this converter.

First, two modules are connected in parallel at battery side. Then the current of each module is reduced by half. Since the conduction loss is proportional to the square of the current, the conduction loss of battery side in this converter will be reduced by half. Then the efficiency is increased significantly.

Second, two modules are connected in series at DC bus side. Then the voltage that each module needs to withstand is greatly reduced and the DC voltage gain can be improved.

Third, the converter can operate without voltage sharing and current sharing control. The steady state equivalent model of the bidirectional DC-DC converter is shown in Fig. 12. Take the step-up mode for example, if the buck/boost works at continuous conduction mode (CCM), the equivalent circuit is shown in Fig. 12(a). It is obvious that the DC bus side voltage of each DC-DC module can be expressed as,

$$V_{bus1} = \frac{nV_{bat}}{1-D} = V_{bus2} \tag{1}$$

since the same duty cycle D is used for each module. And the battery side current of each module can be expressed as,

$$-I_{bat1} = nI_1 = n\frac{I_{bus}}{1-D} = nI_2 = -I_{bat2} \tag{2}$$

If the buck/boost works at discontinuous conduction mode (DCM), the equivalent circuit is shown in Fig. 12(b), in which $R_e(D)$ is,

$$R_e(D) = \frac{2Lf}{D^2} \tag{3}$$

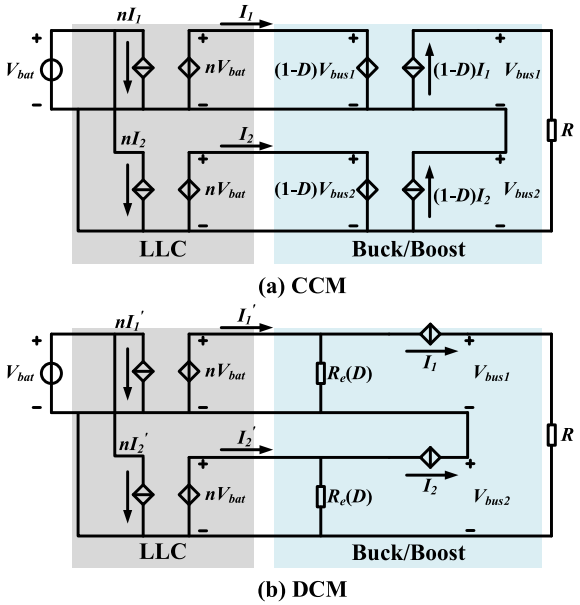

FIGURE 12. The steady state equivalent model of the bidirectional DC-DC converter.

Besides, the equivalent current source can be expressed as,

$$I_1 = \frac{1}{R_e(D)} \frac{n^2 V_{bat}^2}{V_{bus1} - nV_{bat}} = I_2 = \frac{1}{R_e(D)} \frac{n^2 V_{bat}^2}{V_{bus2} - nV_{bat}} \tag{4}$$

It is obvious that

$$\begin{cases} V_{bus1} = V_{bus2} \\ I_1^{'} = I_2^{'} \\ -I_{bat1} = nI_1^{'} = nI_2^{'} = -I_{bat2} \end{cases} \tag{5}$$

Therefore, the separate control for each module is not required and two modules can equalize voltage automatically with the control of DC bus voltage. Furthermore, because the transmission power and battery voltage of the two modules are the same, the two modules can automatically equalize the current on the battery side.

Forth, two modules are identical. Maintenance of the converter will become easier especially in residential situation.

Although the buck/boost is the main object to be controlled in the converter, the isolated bidirectional DC-DC circuit used in the module is the key of the whole converter. To optimize the efficiency of the DC-DC converter, the selection of the isolated bidirectional DC-DC circuit is carried out carefully. It is obvious that DAB and SRC are not suitable for the system since their soft-switching is difficult to achieve at light load. Therefore, LLC and CLLC shown in Fig. 13 will be mainly discussed in the following sections.

B. DESIGN OF BIDIRECTIONAL LLC AND CLLC

The topology of LLC and CLLC are shown in Fig. 10. LLC and CLLC are suitable for the residential photovoltaic generation system because it can achieve soft-switching at any load condition and achieve higher efficiency. Although it is

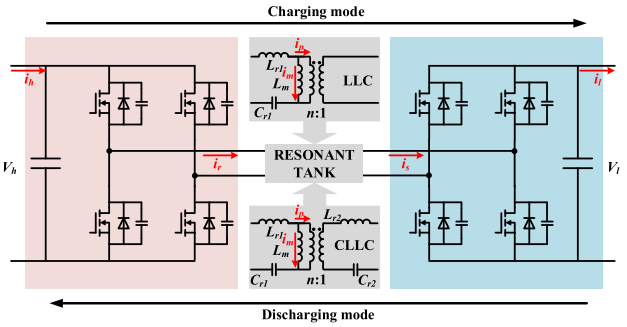

FIGURE 13. Topologies of LLC and CLLC.

difficult to control CLLC for its special voltage gain curve, it can still operate at near resonant frequency as a DCX. Then, comparison of LLC and CLLC is made to select the best topology for the residential photovoltaic power generation system.

The operation principle of bidirectional LLC and CLLC had been introduced in some literatures [22], [27], [29]. Since the isolated bidirectional DC-DC converter in the optimized system is a two-stage topology, the bidirectional LLC or CLLC in this converter can work as a DCX which means that they only operate at resonant frequency. Therefore, the DC voltage gain of LLC and CLLC can be obtained via first harmonic approximation (FHA) and the result can meet the precision requirement near the resonant frequency. Then, to achieve higher efficiency, the bidirectional LLC and CLLC can be designed as follows.

1) DESIGN OF TURN RATIO OF TRANSFORMER

According to FHA, the DC voltage gain of bidirectional LLC, G_{LLC} can be expressed as

$$G_{LLC} = \begin{cases} \dfrac{1}{\sqrt{\dfrac{L_{r1}P^2\pi^4}{64C_{r1}n^4V_l^4}\left(\omega - \dfrac{1}{\omega}\right)^2 + \left(1 + \dfrac{L_{r1}}{L_m} - \dfrac{L_{r1}}{L_m\omega^2}\right)^2}} \\ \qquad \text{(Charging mode)} \\ \dfrac{1}{\sqrt{\dfrac{L_{r1}P^2\pi^4}{64C_{r1}n^4V_l^4}\left(\omega - \dfrac{1}{\omega}\right)^2 + 1}} \\ \qquad \text{(Discharging mode)} \end{cases} \tag{6}$$

In which, L_{r1} is the resonant inductance, C_{r1} is the resonant capacitance, P is the power of LLC, n is the turn ratio of the transformer, L_m is magnetic inductance, V_l is the voltage of battery side and ω is the normalized frequency of bidirectional LLC. It is obvious that the G_{LLC} will be equal to 1 in both charging mode and discharging mode when ω is 1 that switching frequency is equal to the resonant frequency. The same conclusion can be obtained by the expression of G_{CLLC} the DC voltage gain of CLLC (7), as shown at the bottom of the next page. Therefore, to meet the requirement of DC voltage gain, the turn ratio of transformer, n can be expressed

by bus side voltage V_h and battery side voltage V_l as,

$$n = \frac{V_h}{V_l} \tag{8}$$

2) DESIGN OF MAGNETIC INDUCTANCE

Magnetic inductance is an important parameter no matter in LLC or in CLLC. It affects the realization of soft switching and the power loss of the converter. Therefore, the magnetic inductance should be designed carefully.

First, magnetic inductance affects the efficiency of the converter. For LLC, in charging mode, the resonant current i_r, magnetic current i_m, bus side current of transformer i_p and battery side current of transformer i_s can be derived as,

$$i_r(t) = I_r \sin(2\pi f_s t - \varphi) \tag{9}$$

$$i_m(t) = \begin{cases} \dfrac{nV_l t}{L_m} - I_m & 0 \le t \le \dfrac{1}{2f_s} \\ -\dfrac{nV_l\left(t - \frac{1}{2f_s}\right)}{L_m} + I_m & \dfrac{1}{2f_s} < t \le \dfrac{1}{f_s} \end{cases} \tag{10}$$

$$i_p(t) = i_r(t) - i_m(t) \tag{11}$$

$$i_s(t) = -n i_p(t) \tag{12}$$

wherein,

$$\begin{cases} I_m = \dfrac{nV_l}{4L_m f_s} \\ I_r = \sqrt{\left(\dfrac{\pi P}{2nV_l}\right)^2 + I_m^2} \\ \varphi = \arcsin(\dfrac{I_m}{I_r}) \end{cases} \tag{13}$$

In discharging mode, the expression of i_r becomes

$$i_r(t) = -I_r \sin(2\pi f_s t + \pi) \tag{14}$$

$$I_r = \frac{\pi P}{2V_h} \tag{15}$$

For CLLC, in charging mode, the resonant current i_r, magnetic current i_m, bus side current of transformer i_p and battery side current of transformer i_s can be expressed the same as LLC. However, in discharging mode, there are some clear difference in the expression as follows.

$$i_p(t) = I_p \sin(2\pi f_s t - \varphi) \tag{16}$$

$$i_m(t) = \begin{cases} \dfrac{nV_l t}{L_m} - I_m & 0 \le t \le \dfrac{1}{2f_s} \\ -\dfrac{nV_l\left(t - \frac{1}{2f_s}\right)}{L_m} + I_m & \dfrac{1}{2f_s} < t \le \dfrac{1}{f_s} \end{cases} \tag{17}$$

$$i_r(t) = i_p(t) + i_m(t) \tag{18}$$

$$i_s(t) = -n i_p(t) \tag{19}$$

wherein,

$$\begin{cases} I_m = \dfrac{nV_l}{4L_m f_s} \\ I_p = \sqrt{\left(\dfrac{\pi P}{2nV_l}\right)^2 + I_m^2} \\ \varphi = \arcsin(\dfrac{I_m}{I_p}) \end{cases} \tag{20}$$

Thus, the conduction loss and switching loss of LLC and CLLC can be calculated and the relationship between total loss P_{loss} and L_m is shown in Fig. 14. There is an obvious demarcation point in Fig. 14, namely $L_{m.min}$. When L_m is smaller than $L_{m.min}$, the P_{loss} drops rapidly with the increase of L_m, while changes slightly with the increase of L_m when it is greater than $L_{m.min}$. Then $L_{m.min}$ can be set as the minimum value of magnetic inductance,

$$L_m > L_{m,\min} \tag{21}$$

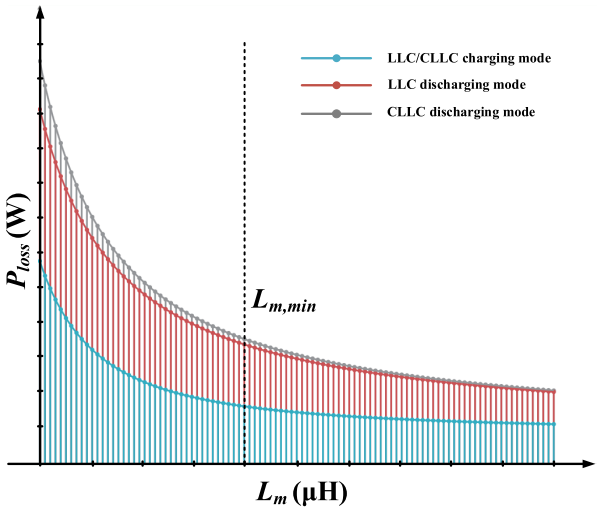

FIGURE 14. Relationship curves between power loss and magnetic inductance in LLC and CLLC.

Second, the realization of soft switching is closely related to the magnetic inductance. Since the LLC or CLLC works at resonant frequency, the battery side can achieve ZCS turn-off naturally. However, the realization of ZVS turn-on in both sides is decided by resonant current during deadtime, which can be approximated as the maximum magnetic current I_m at that time. Then, the soft switching conditions can be expressed as,

$$L_m < \frac{T_d}{8C_{oss}f_s} \tag{22}$$

$$G_{CLLC} = \frac{1}{\sqrt{\frac{L_{r1}^2 P^2 \pi^4}{64 L_m C_{r1} n^4 V_l^4}\left[\left(\frac{2L_m}{L_{r1}} + 1\right)\omega - \left(\frac{2L_m}{L_{r1}} + 2\right)\frac{1}{\omega} + \frac{1}{\omega^3}\right]^2 + \left(1 + \frac{L_{r1}}{L_m} - \frac{L_{r1}}{L_m \omega^2}\right)^2}} \tag{7}$$

In which T_d is the deadtime, C_{oss} is the sum of output capacitance including the bus side device and the battery side device. Furthermore, L_m can be selected by

$$L_{m,\min} < L_m < \frac{T_d}{8C_{oss}f_s} \tag{23}$$

3) DESIGN OF RESONANT COMPONENTS

For LLC and CLLC, the resonant frequency can be expressed as

$$f_r = \frac{1}{2\pi\sqrt{L_{r1}C_{r1}}} \tag{24}$$

Thus, if f_r has been determined and L_m has been selected through the method introduced above, the curves of DC voltage gain of LLC and CLLC at a specific power rating are determined by resonant inductance L_r only. According to (6) and (7), to obtain a relatively flat curve of DC voltage gain, the L_r should be much smaller than L_m, such as one-tenth, to avoid gain variations due to the disturbances of switching frequency and inconsistencies of resonant components. After that, the resonant capacitance can be deduced from the resonant frequency.

TABLE 2. Parameters of LLC and CLLC.

Parameters	LLC	CLLC
Rated Power P_n	2kW	2kW
DC bus side voltage V_h	360V	360V
Battery side voltage V_l	24V	24V
Magnetic inductance L_m	140μH	140μH
Resonant inductance L_{r1}, L_{r2}	14μH	14μH, 62nH
Resonant capacitance C_{r1}, C_{r2}	180nF	180nF, 40.5μF
Turn ratio of transformer n	15	15
Resonant frequency f_r	100kHz	100kHz
Switching frequency f_s	100kHz	100kHz
DC bus side switching devices	STW56N60DM2	STW56N60DM2
Battery side switching devices	BSC014N04LS (8 parallel)	BSC014N04LS (8 parallel)

For CLLC, there are still two components needing to be designed. To obtain the same resonant frequency as bus side and the symmetric equivalent circuit, L_{r2} and C_{r2} can be calculated as

$$\begin{cases} L_{r2} = \dfrac{L_{r1}}{n^2} \\ C_{r2} = n^2 C_{r1} \end{cases} \tag{25}$$

C. COMPARISON OF BIDIRECTIONAL LLC AND CLLC

To compare the two circuits, an LLC and a CLLC circuit were designed to facilitate the analysis of characteristics of these two topologies. The specification is based on the residential photovoltaic power generation system. The battery side voltage V_l is 24V, the bus side voltage V_h is 360V, and P_n, the rated power is 2kW. Then, parameters of two circuits are designed based on the method and are shown in TABLE 2. Thus, the power loss of switching devices in both modes can be calculated.

Besides, to minimize the error of calculated total power loss, the power loss of resonant capacitors and magnetic component are considered. Eight capacitors are parallel connected in the LLC and CLLC and the total equivalent series resistance (ESR) is 50mΩ. However, the resonant capacitance of battery side in CLLC is up to 40.5μF. The selection of the capacitor is very difficult because of large current and high switching frequency, even though the required voltage rating is very low. To minimize the number of capacitors, the capacitance of a single capacitor cannot be too small. Finally, forty-one capacitors are used and total ESR is 0.488mΩ. Then the calculated efficiency curve and loss break down at full load are obtained and shown in Fig. 15 and Fig. 16. The highest efficiency of LLC and CLLC under charging mode and discharging mode are 98.4%, 98.2%, 98.2% and 97.8% respectively. It is obvious that the efficiency of LLC is always slightly higher than CLLC, no matter in charging mode or discharging mode. Fig. 16 shows that the addition of resonant capacitors in the battery side increases the loss of CLLC, which is the main reasons of lower efficiency of CLLC. Although the parallel capacitors greatly reduce the overall ESR, the power loss is still significant because of large current.

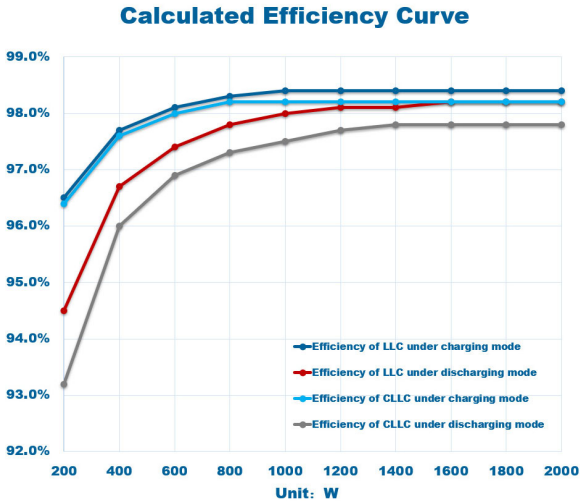

FIGURE 15. Calculated efficiency curves of LLC and CLLC under charging mode and discharging mode respectively.

In addition, too many resonant capacitors are used to meet the capacitance requirement and current rating requirement. The power density is difficult to be further improved.

Besides the efficiency, the resistance of DC voltage gain to frequency disturbance is also a main factor to be considered. According to the FHA, the DC voltage gain of LLC and

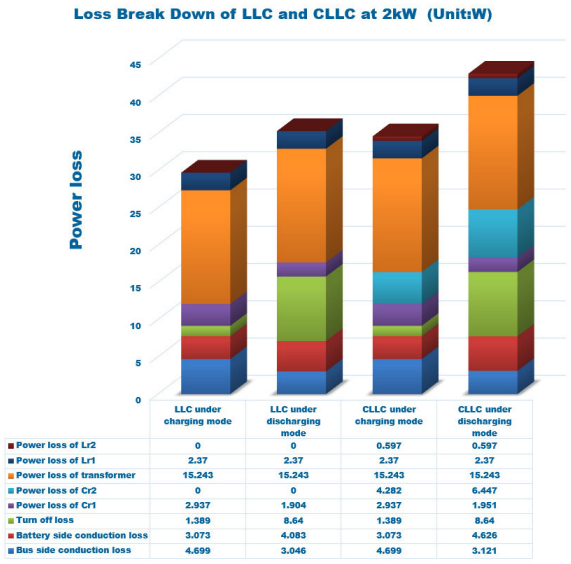

	LLC under charging mode	LLC under discharging mode	CLLC under charging mode	CLLC under discharging mode
Power loss of Lr2	0	0	0.597	0.597
Power loss of Lr1	2.37	2.37	2.37	2.37
Power loss of transformer	15.243	15.243	15.243	15.243
Power loss of Cr2	0	0	4.282	6.447
Power loss of Cr1	2.937	1.904	2.937	1.951
Turn off loss	1.389	8.64	1.389	8.64
Battery side conduction loss	3.073	4.083	3.073	4.626
Bus side conduction loss	4.699	3.046	4.699	3.121

FIGURE 16. Loss break down of LLC and CLLC under charging mode and discharging mode respectively.

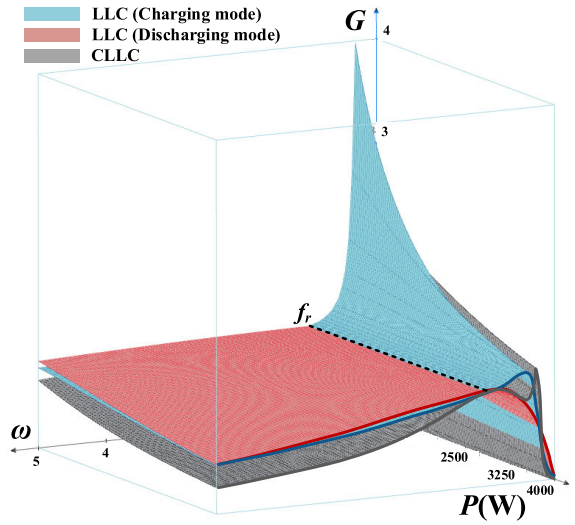

FIGURE 17. Surface of DC voltage gain of LLC and CLLC.

CLLC can be respectively expressed as (6) and (7). The surfaces of DC voltage gain of LLC and CLLC are shown in Fig. 17. It can be seen that the DC voltage gain of CLLC near resonant frequency of CLLC becomes more sensitive to frequency disturbance as the power increases. Therefore, CLLC is not suitable for DCX condition.

In conclusion, LLC is a better topology as bidirectional isolated DC-DC circuit in the residential photovoltaic power generation system, because of: 1) Higher efficiency no matter under charging mode or discharging mode. 2) Higher power density to be further improved. 3) High resistance to frequency disturbance in DCX condition.

Therefore, the LLC is selected in the final scheme to optimize the residential photovoltaic power generation system. The experimental result is introduced in the next section.

V. EXPERIMENTAL RESULT AND ANALYSIS

A. EXPERIMENTAL SYSTEM

In order to optimize the residential photovoltaic power generation system and to verify the design method and conclusions obtained above, a derating experimental platform was set up in the laboratory, DC bus of which is 800V. The configuration of experimental platform is shown in Fig. 18. The coordination of the residential photovoltaic power generation system is controlled by a DSP and a CPLD, TMS320F28377D (TI) and XC2C256 (XILINX), as shown in Fig. 19.

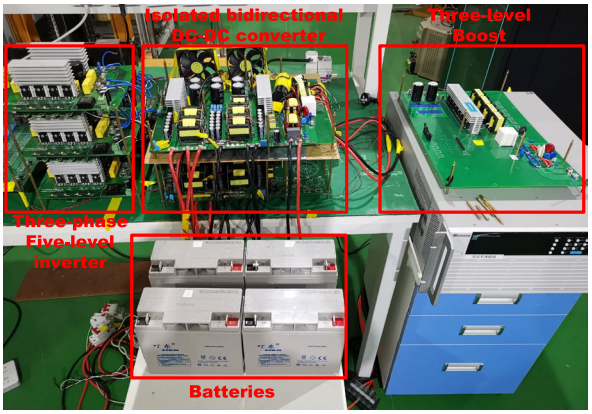

FIGURE 18. The configuration of experimental platform.

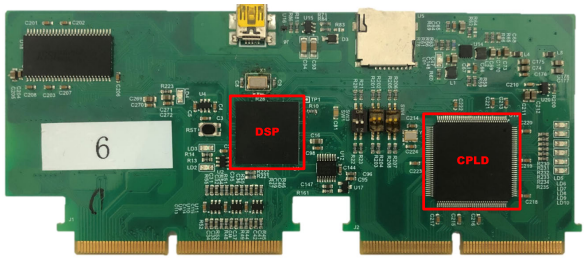

FIGURE 19. The master control board of the system.

As shown in Fig. 18, the system includes a PV emulator, a three-level boost converter, batteries, an isolated bidirectional DC-DC converter and a three-phase five-level converter. And the isolated bidirectional DC-DC converter designed based on the method introduced last section is shown in Fig. 20. The rated power of the isolated bidirectional DC-DC converter is 4kW. Each module is 2kW. The battery side voltage is 24V and DC bus side voltage is 400V. The controller of each converter is TMS320F28069 as shown in Fig. 21. To verify the results of theoretical analysis, the bidirectional DC-DC module is tested at different load condition. Besides, the operation performance of the optimized system is tested.

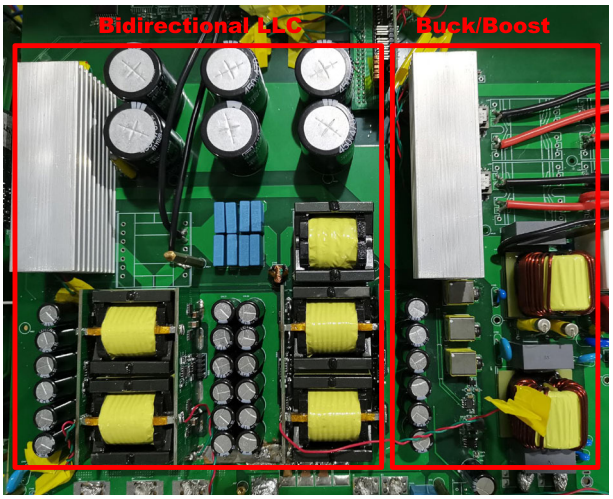

FIGURE 20. The isolated bidirectional DC-DC module in the proposed system.

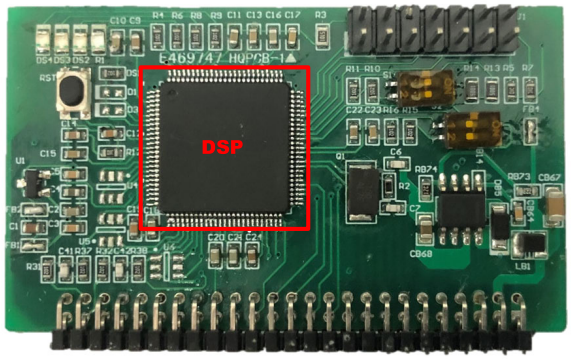

FIGURE 21. The slave control board of each converter.

B. EXPERIMENTAL RESULT AND ANALYSIS

The experimental result of the operation conditions of bidirectional LLC at different load conditions under charging mode has been shown in Fig. 22. In Fig. 22, CH1 is the drive voltage of the DC bus side, CH2 is the voltage between drain and source of switching devices in the DC bus side, CH3 is the drain-source voltage of the devices in the battery side and CH4 is resonant current of the resonant inductor. It is obvious that the body diode of devices has been conducted before its drive voltage turn to high and the ZVS-on has been achieve in the bus side no matter what the load condition is. That is important to optimize the efficiency of the isolated bidirectional DC-DC converter and the proposed system.

The experimental result of the operation conditions of bidirectional LLC at different load conditions under discharging mode has been shown in Fig. 23. In Fig. 23, CH1 is the drain-source voltage of device in the DC bus side, CH2 is the current of transformer in the DC bus side, CH3 is the drive voltage of devices in the battery side and CH4 is resonant current of the resonant inductor. It is obvious that the current of transformer is still greater than 0 at the moment that the drive

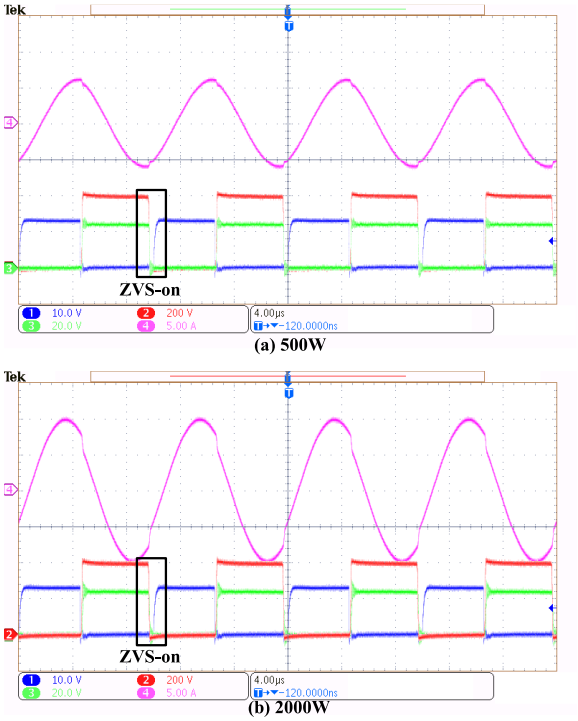

FIGURE 22. The waveforms of bidirectional LLC at different load conditions under charging mode.

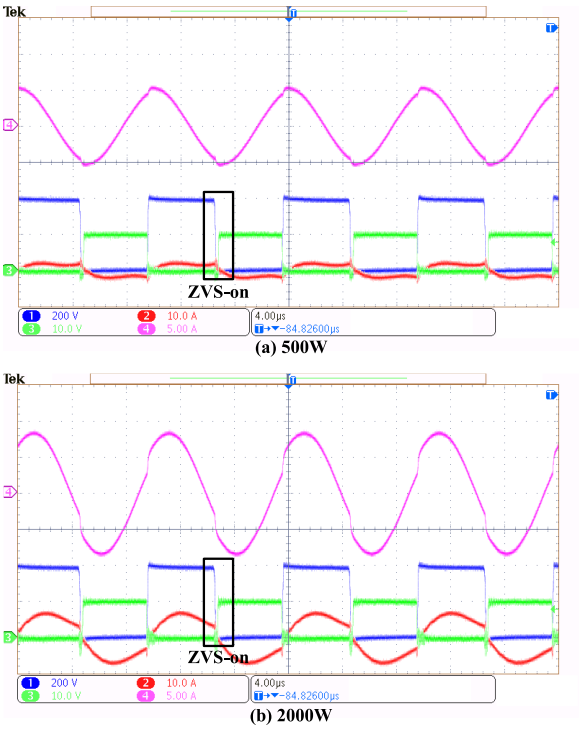

FIGURE 23. The waveforms of bidirectional LLC at different load conditions under discharging mode.

voltage of battery side has turned to high and the ZVS-on has been achieved in the battery side no matter what the load condition is. It is important to optimize the efficiency of

the isolated bidirectional DC-DC converter and the proposed system.

Besides, the experimental result of bidirectional buck/boost converter at full load condition has been shown in Fig. 24. Fig. 24 includes the waveforms of current and drive voltage of the buck/boost converter which has been labeled in the Fig. 24.

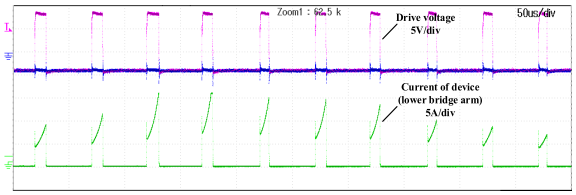

FIGURE 24. The waveforms of buck/boost.

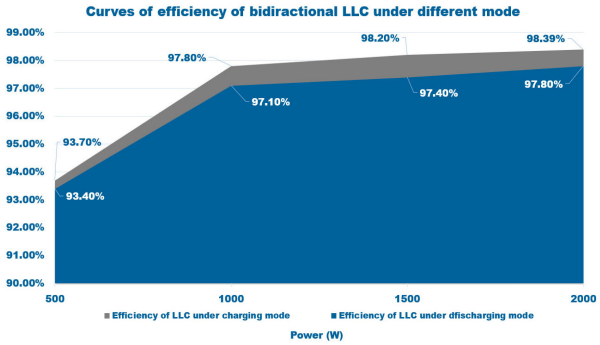

FIGURE 25. The curves of bidirectional LLC under charging and discharging mode.

Then, the experimental results of efficiency of bidirectional LLC and the isolated bidirectional DC-DC module are shown in the Fig. 25 and Fig. 26. Fig. 25 shows the efficiency curves of the bidirectional LLC under charging mode and discharging mode. The designed bidirectional LLC obtains the highest efficiency at full load condition, which is up to 98.39% under charging mode and 97.8% under charging mode. It is obvious that the efficiency of bidirectional LLC under charging mode is always slightly higher than the efficiency under discharging mode which is the same as the theoretical analysis above. It is because that many devices are connected parallel to meet the current and conduction loss requirement at battery side which cause a larger switching loss. The efficiency of bidirectional LLC is approximate to the calculated efficiency shown in the Fig. 10, especially at full load condition. Thus, the loss break down of the bidirectional LLC shown in Fig. 16 is validated. Fig. 26 shows the efficiency curves of the isolated bidirectional DC-DC module under charging mode and discharging mode separately. The efficiency of isolated bidirectional DC-DC module can achieve 97.5% and 96.03% at 2500W under charging mode and discharging mode. It is because the power loss of bidirectional LLC is much reduced and buck/boost can achieve high efficiency that may higher than 99% even though it is a hard-switching circuit.

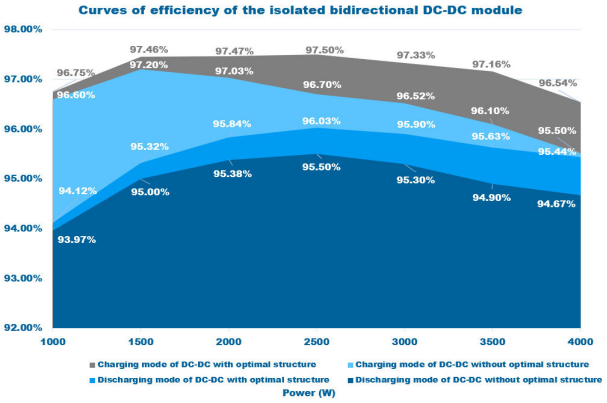

FIGURE 26. The curves of the isolated bidirectional DC-DC module and comparison with the DC-DC converter without optimization.

FIGURE 27. The prototype of the DC-DC converter without optimal structure.

Besides, efficiency curves of the isolated bidirectional DC-DC converter without optimal structure under charging mode and discharging mode are also listed in Fig. 26. The prototype of this DC-DC converter is designed following the method proposed above and is shown in Fig. 27. At full load condition, the efficiency of optimized DC-DC converter can achieve 96.54% and 95.44%. It is nearly 1% higher than the DC-DC converter without optimal structure. Besides, it is obvious that the greater the output power is, the greater the efficiency improvement will be no matter under charging mode or discharging mode. This is because that the optimal structure proposed in the paper can effectively reduce the current and conduction loss.

The experimental result of current sharing characters of the isolated bidirectional DC-DC converter has been shown in Fig. 28. In Fig. 28, CH1 is the battery side current of module-I and CH4 is the battery side current of module-II tested at the full load condition. The difference between the two currents is 1.6A, only 0.98% of the total current.

The experimental result of mode switching of one module of the isolated bidirectional DC-DC converter has been shown in Fig. 29, which includes waveforms of battery voltage, battery current, DC bus voltage and DC bus current as labeled in the Fig. 29. When the mode switches from charging to

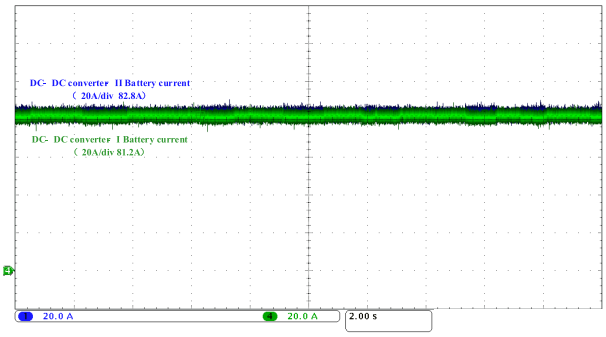

FIGURE 28. The waveforms of current sharing of the isolated bidirectional DC-DC converter without separate control.

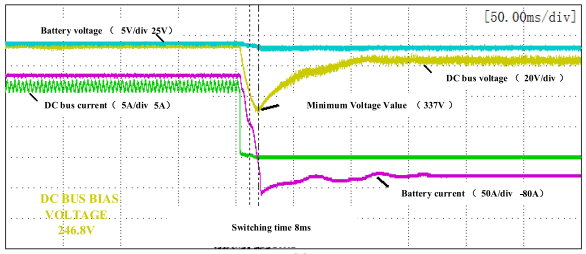

(a) From charging mode to discharging mode

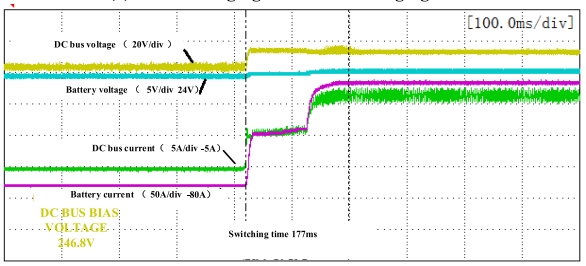

(b) From discharging mode to charging mode

FIGURE 29. The waveforms of isolated bidirectional DC-DC module at switching time.

discharging, the switching time is 8ms. During the switching process, the maximum voltage of the DC bus side is 337V and the DC bus voltage is 674V. At that time, the DC-AC converter can work well. When the mode switches from discharging to charging, the switching time is 177ms. There is no abnormality in the waveforms. During these two switching processes, the DC-AC converter works well and the system can operate stably.

The experimental results of three-phase five-level DC-AC converter have been shown in Fig. 30 and Fig. 31. Fig. 30 shows the result of singe phase in the DC-AC converter, in which CH2 is output voltage of the DC-AC converter, CH3 is line voltage and CH4 is line current at full load condition. Five-level DC-AC converter can reduce the THD and EMI noise and increase the DC bus voltage and efficiency of the system. Fig. 31 shows the line current of the inverter when the DC bus voltage is controlled by the DC-AC converter. CH1 is the voltage of DC bus, CH2 is the line current of phase A and CH3 is the line current of phase B.

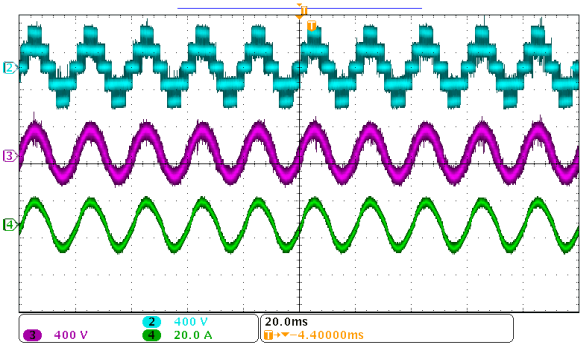

FIGURE 30. The waveforms of the five-level DC-AC converter.

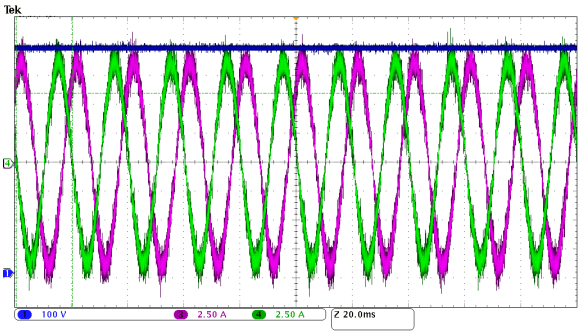

FIGURE 31. The waveforms of the three-phase five-level DC-AC converter.

It is obvious that at that condition the DC bus voltage can be controlled well.

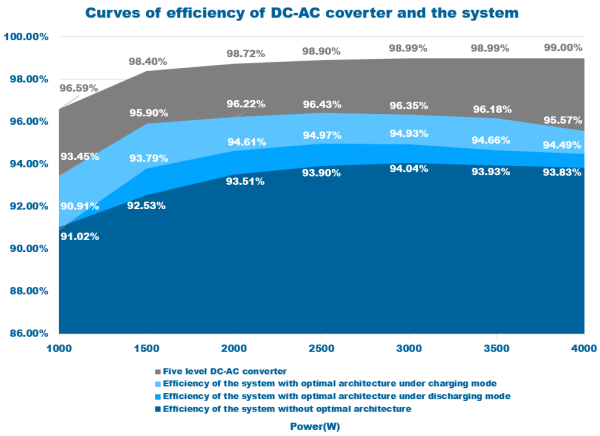

FIGURE 32. The curves of efficiency of the five-level DC-AC converter and the whole system.

Fig. 32 shows the efficiency of the five-level DC-AC converter in the system. Besides, the curves of the whole system are also shown in Fig. 32. There are three curves of the system and the last one is the efficiency of the system without optimal architecture. This system employed the 400V DC bus and single-phase two-level DC-AC converter. Besides, the bidirectional DC-DC converter used a traditional structure. The highest efficiency of the optimized system

can achieve 96.43% and 94.97% under charging mode and discharging mode. It is obvious, the efficiency of the system can be improved a lot because of the optimal architecture.

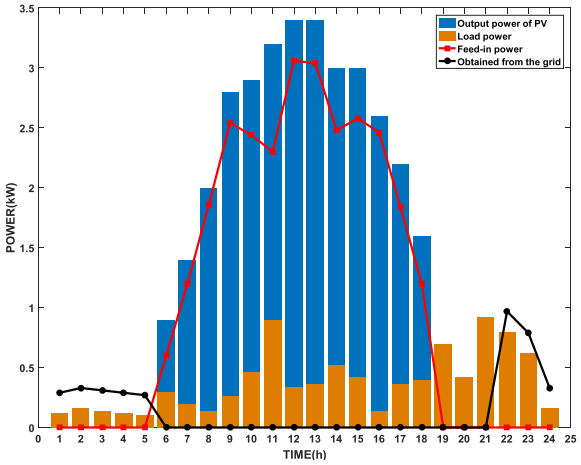

FIGURE 33. Distribution of typical daily power consumption of a household in Shanghai.

TABLE 3. Parameters of the residential photovoltaic power generation system.

Parameters	Value
Rated Power	4kW
Battery capacity	10kW·h
State subsidy	¥0.42/(kW·h)
Local subsidy	¥0.4/(kW·h)
Feed-in tariff	¥0.42/(kW·h)
Peak hour tariff	¥0.62/(kW·h) (6:00~22:00)
Valley hour tariff	¥0.62/(kW·h) (22:00~6:00)

Fig. 33 shows the typical power consumption of a household and daily output power of PV in Shanghai. Fig. 33 is obtained from a 4kW PV system with a 10kW·h BESS. The parameters of the residential photovoltaic power generation system have been shown in TABLE 3. According to Fig. 33, the output energy of the PV is 33.1kW·h. Then, the state subsidy and local subsidy in Shanghai is ¥13.90 and ¥13.24 separately. The total energy residential load consumed is 9.22kW·h, in which 6.02 kW·h is provided by PV or BESS and the others is provided by the grid under valley hour tariff. It is because that in the proposed energy management scheme the batteries are not allowed to be charged to obtain higher economic benefits. Therefore, ¥3.73 is saved and ¥1.43 is fees of electricity in a whole day which has included the fees for batteries charging. The feed-in energy in such a day is 27.56kW·h and the economic benefits is ¥11.58. Therefore, the total economic benefit is ¥41.02. Compared with the conventional energy management scheme without the consideration of the ToU tariff introduced in [2], the economic benefit can be increased by 1.5%. In addition, in the case of serious shortage of photovoltaic power generation, such as rainy days, the total economic benefit of conventional energy management scheme is fuzzy. It is because that the SOC may lower than 5% during peak hour and the batteries may be charged in a higher tariff.

According to the experimental results and analysis above, the optimized residential photovoltaic power generation system can be implemented and work well with higher efficiency and higher economic benefits. The isolated bidirectional DC-DC converter can achieve higher efficiency and reliability in the system.

VI. CONCLUSION

This paper dedicates to optimize the residential photovoltaic power generation system. The optimized system oriented to 1500V DC bus is proposed. The higher DC bus voltage greatly reduces line loss and improves efficiency of the system. To improve the reliability of power supply and increase the economic benefits, an energy management scheme is proposed. Sunlight hours and ToU tariff are considered. The scheme ensures the reliability of power supply for the residential load, meanwhile reducing the economic cost by reducing grid power supply. To optimize the performance of the converters in the system, the optimized method for the structure of bidirectional dc-dc converter is proposed. This structure can easily achieve higher DC voltage gain and efficiency to further optimize the system. According to the experimental results, the highest efficiency of the isolated bidirectional DC-DC converter can achieve 97.50% under charging mode and 96.03% under discharging mode. Furthermore, for low battery voltage situation in the residential system, LLC and CLLC under DCX mode are evaluated and the optimized design method is proposed. The efficiency at different load conditions and loss break down of LLC and CLLC are calculated. In low battery voltage application, the LLC is a better topology which is selected in the system and its efficiency can achieve 98.39% and 97.80% under charging mode and discharging mode separately. The optimized system can improve the efficiency significantly and economic benefits can be increased.

REFERENCES

[1] Y. Wang, X. Lin, and M. Pedram, "A near-optimal model-based control algorithm for households equipped with residential photovoltaic power generation and energy storage systems," *IEEE Trans. Sustain. Energy*, vol. 7, no. 1, pp. 77–86, Jan. 2016.

[2] R. Li, X. Liang, X. Li, and X. Cai, "On/off-grid integrated photovoltaic power generation system," in *Proc. Int. Power Electron. Appl. Conf. Expo.*, Shanghai, China, Nov. 2014, pp. 255–259.

[3] U. Akram, M. Khalid, and S. Shafiq, "An improved optimal sizing methodology for future autonomous residential smart power systems," *IEEE Access*, vol. 6, pp. 5986–6000, 2018.

[4] G. G. Talapur, H. M. Suryawanshi, L. Xu, and A. B. Shitole, "A reliable microgrid with seamless transition between grid connected and islanded mode for residential community with enhanced power quality," *IEEE Trans. Ind. Appl.*, vol. 54, no. 5, pp. 5246–5255, Sep. /Oct. 2018.

[5] J. Pahasa and I. Ngamroo, "Coordinated PHEV, PV, and ESS for microgrid frequency regulation using centralized model predictive control considering variation of PHEV number," *IEEE Access*, vol. 6, pp. 69151–69161, 2018.
[6] D. Casadei, G. Grandi, and C. Rossi, "Single-phase single-stage photovoltaic generation system based on a ripple correlation control maximum power point tracking," *IEEE Trans. Energy Convers.*, vol. 21, no. 2, pp. 562–568, Jun. 2006.
[7] T. Shimizu, O. Hashimoto, and G. Kimura, "A novel high-performance utility-interactive photovoltaic inverter system," *IEEE Trans. Power Electron.*, vol. 18, no. 2, pp. 704–711, Mar. 2003.
[8] W. Li and X. He, "Review of nonisolated high-step-up DC/DC converters in photovoltaic grid-connected applications," *IEEE Trans. Ind. Electron.*, vol. 58, no. 4, pp. 1239–1250, Apr. 2011.
[9] K. Sun, L. Zhang, Y. Xing, and J. M. Guerrero, "A distributed control strategy based on DC bus signaling for modular photovoltaic generation systems with battery energy storage," *IEEE Trans. Power Electron.*, vol. 26, no. 10, pp. 3032–3045, Oct. 2011.
[10] Y. Chen, G. Xie, and R. Li, "Reducing energy consumption with cost budget using available budget preassignment in heterogeneous cloud computing systems," *IEEE Access*, vol. 6, pp. 20572–20583, 2018.
[11] V. T. Tran, K. M. Muttaqi, and D. Sutanto, "A robust power management strategy with multi-mode control features for an integrated PV and energy storage system to take the advantage of ToU electricity pricing," *IEEE Trans. Ind. Appl.*, vol. 55, no. 2, pp. 2110–2120, Mar./Apr. 2019.
[12] S. T. Kim, S. Bae, Y. C. Kang, and J. W. Park, "Energy management based on the photovoltaic HPCS with an energy storage device," *IEEE Trans. Ind. Electron.*, vol. 62, no. 7, pp. 4608–4617, Jul. 2015.
[13] C. Jain and B. Singh, "An adjustable DC link voltage based control of multifunctional grid interfaced solar PV system," *IEEE J. Emerg. Sel. Topics Power Electron.*, vol. 5, no. 2, pp. 651–660, Jun. 2017.
[14] N. Mahmud, A. Zahedi, and A. Mahmud, "A cooperative operation of novel PV inverter control scheme and storage energy management system based on ANFIS for voltage regulation of grid-tied PV system," *IEEE Trans. Ind. Informat.*, vol. 13, no. 5, pp. 2657–2668, Oct. 2017.
[15] R. Carbone, "Grid-connected photovoltaic systems with energy storage," in *Proc. Int. Conf. Clean Elect. Power*, Jun. 2009, pp. 760–767.
[16] W. Libo, Z. Zhengming, and L. Jianzheng, "A single-stage three-phase grid-connected photovoltaic system with modified MPPT method and reactive power compensation," *IEEE Trans. Energy Convers.*, vol. 22, no. 4, pp. 881–886, Dec. 2007.
[17] G. Grandi, C. Rossi, D. Ostojic, and D. Casadei, "A new multilevel conversion structure for grid-connected PV applications," *IEEE Trans. Ind. Electron.*, vol. 56, no. 11, pp. 4416–4426, Nov. 2009.
[18] J.-S. Kim, J.-M. Kwon, and B.-H. Kwon, "High-efficiency two-stage three-level grid-connected photovoltaic inverter," *IEEE Trans. Ind. Electron.*, vol. 65, no. 3, pp. 2368–2377, Mar. 2018.
[19] X. Guo, M. C. Cavalcanti, A. M. Farias, and J. M. Guerrero, "Single-carrier modulation for neutral-point-clamped inverters in three-phase transformerless photovoltaic systems," *IEEE Trans. Power Electron.*, vol. 28, no. 6, pp. 2635–2637, Jun. 2013.
[20] Y. Shi, L. Wang, R. Xie, Y. Shi, and H. Li, "A 60-kW 3-kW/kg five-level T-type SiC PV inverter with 99.2% peak efficiency," *IEEE Trans. Ind. Electron.*, vol. 64, no. 11, pp. 9144–9154, Nov. 2017.
[21] S. Jadhav, N. Devdas, S. Nisar, and V. Bajpai, "Bidirectional DC-DC converter in solar PV system for battery charging application," in *Proc. Int. Conf. Smart City Emerg. Technol. (ICSCET)*, Mumbai, India, Jan. 2018, pp. 1–4.
[22] F. Shi, R. Li, J. Yang, and W. Yu, "High efficiency bidirectional DC-DC converter with wide gain range for photovoltaic energy storage system utilization," in *Proc. IEEE Int. Power Electron. Appl. Conf. Expo. (PEAC)*, Shenzhen, China, Nov. 2018, pp. 1–6.
[23] H. Bai, and C. Mi, "Eliminate reactive power and increase system efficiency of isolated bidirectional dual-active-bridge DC-DC converters using novel dual-phase-shift control," *IEEE Trans. Power Electron.*, vol. 23, no. 6, pp. 2905–2914, Nov. 2008.
[24] C. Mi, H. Bai, C. Wang, and S. Gargies, "Operation, design and control of dual H-bridge-based isolated bidirectional DC-DC converter," *IET Power Electron.*, vol. 1, no. 4, pp. 507–517, 2008.
[25] X. Li and A. K. S. Bhat, "Analysis and design of high-frequency isolated dual-bridge series resonant DC/DC converter," *IEEE Trans. Power Electron.*, vol. 25, no. 4, pp. 850–862, Apr. 2010.
[26] G. Ortiz, D. Bortis, J. W. Kolar, and O. Apeldoorn, "Soft-switching techniques for medium-voltage isolated bidirectional DC/DC converters in solid state transformers," in *Proc. 38th Annu. Conf. IEEE Ind. Electron. Soc.*, Oct. 2012, pp. 5233–5240.
[27] X. Fang, H. Hu, Z. J. Shen, and I. Batarseh, "Operation mode analysis and peak gain approximation of the LLC resonant converter," *IEEE Trans. Power Electron.*, vol. 27, no. 4, pp. 1985–1995, Apr. 2012.
[28] T. Jiang, J. Zhang, X. Wu, K. Sheng, and Y. Wang, "A bidirectional LLC resonant converter with automatic forward and backward mode transition," *IEEE Trans. Power Electron.*, vol. 30, no. 2, pp. 757–770, Feb. 2015.
[29] J.-H. Jung, H.-S. Kim, M.-H. Ryu, and J.-W. Baek, "Design methodology of bidirectional CLLC resonant converter for high-frequency isolation of DC distribution systems," *IEEE Trans. Power Electron.*, vol. 28, no. 4, pp. 1741–1755, Apr. 2013.
[30] W. Chen, P. Rong, and Z. Lu, "Snubberless bidirectional DC-DC converter with new CLLC resonant tank featuring minimized switching loss," *IEEE Trans. Ind. Electron.*, vol. 57, no. 9, pp. 3075–3086, Sep. 2010.
[31] H. Li, L. Bai, Z. Zhang, S. Wang, J. Tang, X. Ren, and J. Li, "A 6.6kW SiC bidirectional on-board charger," in *Proc. IEEE Appl. Power Electron. Conf. Expo. (APEC)*, San Antonio, TX, USA, Mar. 2018, pp. 1171–1178.
[32] Z. U. Zahid, Z. M. Dalala, R. Chen, B. Chen, and J.-S. Lai, "Design of bidirectional DC-DC resonant converter for vehicle-to-grid (V2G) applications," *IEEE Trans. Transp. Electrific.*, vol. 1, no. 3, pp. 232–244, Oct. 2015.

RUI LI (S'10–M'11) received the Ph.D. degree in electrical engineering from Zhejiang University, Hangzhou, China, in 2010.

From 2008 to 2009, he was an Academic Guest with the Power Electronic Systems Laboratory, Swiss Federal Institute of Technology, Zürich, Switzerland. From 2014 to 2015, he was a Postdoctoral Research Scholar with the Center for Advanced Power Systems, Department of Electrical and Computer Engineering, College of Engineering, Florida State University, Tallahassee, FL, USA. Since 2010, he has been with the Department of Electrical Engineering, School of Electronics, Information and Electrical Engineering, Shanghai Jiao Tong University, Shanghai, China, where he is currently an Associate Professor. His current research interests include the application of power electronics in renewable energy conversion. He was a recipient of the IEEE Power Electronics Society Transactions Second Prize Paper Award, in 2015.

FANGYUAN SHI received the bachelor's degree in electrical engineering from Shanghai Maritime University, Shanghai, China, in 2017. He is currently pursuing the master's degree with the Key Laboratory of Control of Power Transmission and Conversion, Ministry of Education, School of Electronic Information and Electrical Engineering, Shanghai Jiao Tong University, China.

His current research interests include high-efficiency and high power-density bidirectional dc–dc converters.